

Stabilizer Entanglement as a Magic Highway

Zong-Yue Hou,¹ ChunJun Cao,^{2,*} and Zhi-Cheng Yang^{1,3,†}

¹*School of Physics, Peking University, Beijing 100871, China*

²*Department of Physics, Virginia Tech, Blacksburg, VA, USA 24061*

³*Center for High Energy Physics, Peking University, Beijing 100871, China*

(Dated: March 28, 2025)

Non-stabilizerness is a key resource for fault-tolerant quantum computation, yet its interplay with entanglement in dynamical settings remains underexplored. We study a well-controlled, analytically tractable setup that isolates entanglement generation from magic injection. We analytically and numerically demonstrate that stabilizer entanglement functions as a highway that facilitates the spreading of locally injected magic throughout the entire system. Specifically, for an initial stabilizer state with bipartite entanglement E , the total magic growth, quantified by the linear stabilizer entropy Y , follows $\bar{Y} \propto 2^{-|A|-E}$ under a Haar random unitary on a local subregion A . Moreover, when applying a tensor product of local Haar random unitaries, the resulting state's global magic approaches that of a genuine Haar random state if the initial stabilizer state is sufficiently entangled by a system-size-independent amount. Similar results are also obtained for tripartite stabilizer entanglement. We further extend our analysis to non-stabilizer entanglement and magic injection via a shallow-depth brickwork circuit, and find that the qualitative picture of our conclusion remains unchanged.

Introduction.- Understanding what distinguishes quantum systems from classical ones has been a challenging and multi-faceted endeavor. Much of the impact of quantumness in physics has been focusing on the idea of quantum entanglement, which played a central role in characterizing topological order [1–3], dynamically induced phases [4], quantum chaos, and even the emergence of spacetime [5]. However, entanglement being a quantum correlation, is just one facet of quantumness. Quantum advantage, for example, is concerned with the hardness of simulating quantum systems on a classical computer. This facet is distinct from entanglement as many highly entangled systems prepared using Clifford operations violate Bell's inequalities but can be efficiently simulated classically [6, 7]. The notion of classical hardness therefore constitutes a second layer of quantumness and is intimately connected to non-stabilizerness or magic [8–13].

Like entanglement, magic is an important but distinct quantum resource for realizing fault-tolerant *universal* quantum computation [13, 14]. Therefore, it is crucial to understand any physical consequences played by this orthogonal dimension to entanglement in quantum systems. The importance of non-stabilizerness has been largely overlooked in quantum many-body physics until recently, where a flurry of activities have been dedicated to study its total extent in various systems, which has implication for resource estimation in state preparation and quantum simulation [15–18], in characterizing phase transitions [19, 20], in quantum dynamics [21–24], in improved quantum simulation with tensor networks [25, 26], and in quantum gravity [27, 28]. Arguably, the most fascinating perspective comes from the interplay between magic and entanglement [28–32] as both are needed for

quantum advantage.

Recent work revealed that, unlike the spread of entanglement which takes time linear in system size in spatially local Haar random circuits, magic appears to saturate in $O(\log n)$ time [33] (whereas it spreads much more slowly in Hamiltonian systems [34]). In the long time limit, it is also understood that magic in these highly entangled system is similar to the scrambling/encoding of information in quantum error correcting codes where it quickly delocalizes and can only be found when one can access a large part of the system [24, 35, 36]. This asymptotic behavior is consistent with the observation that subsystem magic quickly rises and decays to almost zero as a state thermalizes [22].

Despite these preliminary findings, the fundamental mechanisms underlying magic dynamics, particularly the interplay between magic injection and entanglement, remain poorly understood. Specifically, the role of entanglement in facilitating the growth and spread of magic, and vice versa, is yet to be determined in a quantitative manner. In generic quantum circuits and Hamiltonian dynamics, this interplay is inherently complex, as each time step of evolution simultaneously injects magic and increases entanglement [33, 37]. To gain deeper insights into magic dynamics, a well-controlled setup that isolates different contributing factors is essential. Here we study precisely one such setting and show that entanglement, or at least stabilizer entanglement, acts as a conduit for magic, allowing it to spread much faster to parts of the system that are entangled. This would constitute an important first step in understanding how magic dynamics is distinct and yet interlinked with various types of entanglement dynamics.

In this work, we analytically and numerically demonstrate that, given an initial stabilizer state with bipartite entanglement E , the total growth of magic, as quantified by the linear stabilizer entropy Y under magic in-

* cjcao@vt.edu

† zcyang19@pku.edu.cn

jection via a Haar-random unitary acting on a local subregion A , is enhanced by the presence of entanglement: $Y \propto 2^{-|A|-E}$. Furthermore, when a unitary of the form $U = U_A \otimes U_B$, consisting of independently Haar-random local unitaries on subsystems A and B , is applied, the global magic of the resulting state becomes nearly indistinguishable from that of a fully Haar-random state, provided the initial state is sufficiently entangled. Interestingly, the amount of entanglement necessary for such indistinguishability from Haar random magic is independent of system size. Similar results are also obtained for tripartite stabilizer entanglement. We further extend our analysis to non-stabilizer entanglement and magic injection via a shallow-depth brickwork circuit, and find that the qualitative picture of our conclusion remains unchanged in these cases.

Quantum magic and its measure.— Quantum magic quantifies the amount of “non-stabilizer” or “non-Clifford” resources in a quantum state. A computable measure for quantum magic, which we will primarily focus on in this work, is given by the *linear stabilizer entropy*. Denote by P_N the set of N -qubit Pauli strings. The linear stabilizer entropy for a pure state $\rho = |\psi\rangle\langle\psi|$ is defined as $Y(\rho) := 2^{-N} \sum_{P \in P_N} \text{tr}(P\rho)^4$. To gain some intuition about this quantity, first consider a stabilizer pure state. There are precisely 2^N Pauli strings corresponding to the stabilizer group elements of ρ for which $\text{tr}(P\rho)^4 = 1$, and $\text{tr}(P\rho)^4 = 0$ for all other Pauli strings. Thus $Y(\rho) = 1$ for stabilizer states. For a generic non-stabilizer pure state, the Pauli spectrum satisfies the normalization condition: $2^{-N} \sum_{P \in P_N} \text{tr}(P\rho)^2 = 1$. Therefore, $Y(\rho)$ defined above can be thought of as the second moment of the Pauli spectrum of ρ , which characterizes how delocalized the expectation values of P are over all possible Pauli strings. The linear stabilizer entropy satisfies the following properties: (i) faithfulness: let STAB_n denote the set of all n -qubit pure stabilizer states, then $Y(\rho) = 1$ iff $\rho \in \text{STAB}_n$, otherwise $Y(\rho) < 1$; (ii) invariant under Clifford unitaries U_C : $Y(U_C \rho U_C^\dagger) = Y(\rho)$; (iii) multiplicative: $Y(\rho_A \otimes \rho_B) = Y(\rho_A)Y(\rho_B)$; (iv) the closely related quantity $M^{\text{lin}} := 1 - Y$ is a strong pure-state monotone under free operations [38]. Hence, $Y(\rho)$ serves as a good measure for quantum magic from the point of view of magic-state resource theory. Moreover, the logarithm of $Y(\rho)$ is related to the second stabilizer Rényi entropy $M_2(\rho) = -\log Y(\rho)$, another widely used magic measure [39].

Stabilizer entanglement facilitates magic injection.— To illustrate how stabilizer entanglement can influence magic injection, we examine the effect of a single-qubit T gate on two distinct stabilizer states: an unentangled product state, $|\psi_1\rangle = |+\rangle^{\otimes N} = ((|0\rangle + |1\rangle)/\sqrt{2})^{\otimes N}$, and a GHZ state with long-range entanglement, $|\psi_2\rangle = (|0\rangle^{\otimes N} + |1\rangle^{\otimes N})/\sqrt{2}$. In both cases, the initial states contain no magic, and the T gate injects magic locally. However, the manner in which this injected magic manifests differs significantly between the two cases. In $T|\psi_1\rangle$,

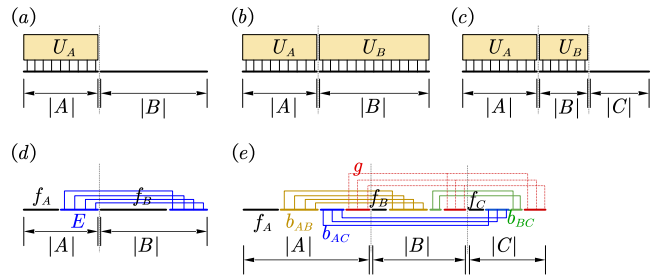


FIG. 1. Schematics of the setup used for analytical and numerical calculations. The initial states are bipartite or tripartite stabilizer pure states. (a) A Haar random unitary injects magic by acting on a subregion A . (b) A factorized unitary $U = U_A \otimes U_B$, where U_A and U_B are independently Haar-random, acts on the initial stabilizer state. (c) A factorized unitary $U = U_A \otimes U_B$ injects magic by acting on subregion AB of a tripartite system. (d) Initial state (2) for numerical simulations of the setup in (a). The state consists of f_A and f_B qubits in $|+\rangle$ state in subsystem A and B , respectively, along with E Bell pairs shared between A and B . (e) Initial state for obtaining Eq. (5). The state initial state consists of g GHZ states shared among A , B , and C ; b_{AB} , b_{AC} , and b_{BC} Bell pairs shared between subsystems AB , AC , and BC , respectively, and f_A , f_B , f_C single-qubit states in each individual subsystem.

the injected magic remains locally accessible and can be directly probed at the specific qubit where the T gate is applied. In contrast, for $T|\psi_2\rangle$, the state appears non-magical to any local observer with access only to a subregion of the system. This simple example illustrates that the propagation of locally injected magic throughout the system is intrinsically tied to the entanglement structure of the initial state.

To further quantify how stabilizer entanglement facilitates magic spreading, we consider the setup illustrated in Fig. 1(a), which enables an analytical calculation. Specifically, we begin with an initial stabilizer pure state $\rho = |\psi\rangle\langle\psi|$, partitioned into subregion A and its complement B . A Haar random unitary U_A is then applied to subregion A , and we are interested in computing the linear stabilizer entropy of the resulting state $\sigma = U_A |\psi\rangle\langle\psi| U_A^\dagger$, averaged over Haar random unitaries. We first make a few remarks on this particular choice of setup before showing the result. This construction is a natural generalization of the toy example discussed above, replacing the single-qubit unitary with a Haar random unitary on a finite subregion. While the Haar-random unitary may appear nonlocal within subregion A , it is local relative to the entire system if $|A| \ll |B|$. The use of Haar random unitaries primarily serves to render the analytical calculations more tractable. We will show below that key qualitative features of our results persist even when considering more structured unitaries within subregion A . Secondly, this setup clearly separates entanglement generation with respect to the bipartition and magic injection. The unitary acting on A injects magic

to the system while preserving the amount of entanglement between A and B , including the full entanglement spectrum. As many, if not most, operationally convenient circuits apply Clifford gates and non-Clifford phase gates in separate stages, e.g. Clifford+T decomposition [13] and the PFC ensemble that prepare pseudorandom unitaries [40], our setup is to probe the internal dynamics that take place between the most elementary layers in those circuits. This is complementary to the random unitary circuit model used in Ref. [33] to study magic saturation. In that model, unitary gates simultaneously generate entanglement and inject magic, leading to universal late-time magic dynamics prior to saturation, regardless of the initial state.

We analytically compute the linear stabilizer entropy $Y(U_A|\psi\rangle\langle\psi|U_A^\dagger)$, averaged over the ensemble of Haar random unitaries U_A . In the limit $|A| \gg 1$, we obtain, to leading order,

$$\bar{Y} = \mathbb{E}_{U_A} Y \left(U_A |\psi\rangle\langle\psi| U_A^\dagger \right) = 4 \cdot 2^{-|A|-E} \left[1 + O(2^{-|A|-E}) \right], \quad (1)$$

where $E = -\text{tr}(\rho_A \log_2 \rho_A)$ is the amount of entanglement between A and B , which is an integer for a stabilizer state $|\psi\rangle$. Eq. (1) establishes a *quantitative* relation between the efficiency of local magic injection and the amount of stabilizer entanglement contained in the target state. For a fixed subregion A , the average $Y(\rho)$ decays exponentially with the amount of entanglement between A and its complement. Therefore, global magic injection on AB is enhanced with entanglement, which acts as a throttle that controls how much magic can flow to region B from A . A detailed derivation of Eq. (1) is provided in the Supplemental Material (SM) [41], yet its qualitative features, particularly the factor $2^{-|A|-E}$ can be understood straightforwardly. Since the unitary acts only on subsystem A , stabilizers supported entirely on B remains unchanged under U_A and contribute to $Y(\rho)$. A simple counting shows that the number of surviving stabilizers is precisely $2^{|B|-E}$, leading to the factor $2^{-|A|-E}$ in Eq. (1). The prefactor 4 in front of $2^{-|A|-E}$ is, in some sense, non-universal. To see this, let us define the generalized linear stabilizer entropy $Y_\alpha(\rho) := 2^{-N} \sum_{P \in P_N} \text{tr}(P\rho)^{2^\alpha}$. Eq. (1) thus corresponds to the specific case $\alpha = 2$. Similarly, $Y_\alpha(\rho)$ is related to the α -th stabilizer Rényi entropy: $M_\alpha(\rho) = \frac{1}{1-\alpha} \log Y_\alpha(\rho)$. In the limit $\alpha \rightarrow \infty$, only the surviving stabilizers supported on B contribute, yielding $\bar{Y}_\infty = 2^{-|A|-E}$. For arbitrary α , we have $\bar{Y}_\alpha = (1 + c_\alpha) 2^{-|A|-E}$, with the one coming from the surviving stabilizers, and c_α being an α -dependent number coming from contributions of all other Pauli strings. Specifically, Eq. (1) implies that for $\alpha = 2$, we have $c_2 = 3$.

To test Eq. (1), particularly the regime of validity of neglecting subleading corrections, we perform numerical simulations of the setup depicted in Fig. 1(a). Recall that any stabilizer state $|\psi\rangle$ can be brought to the form of Eq. (2) by local Clifford unitaries [42]: $|\Phi\rangle = U_A^{\text{Cliff}} \otimes$

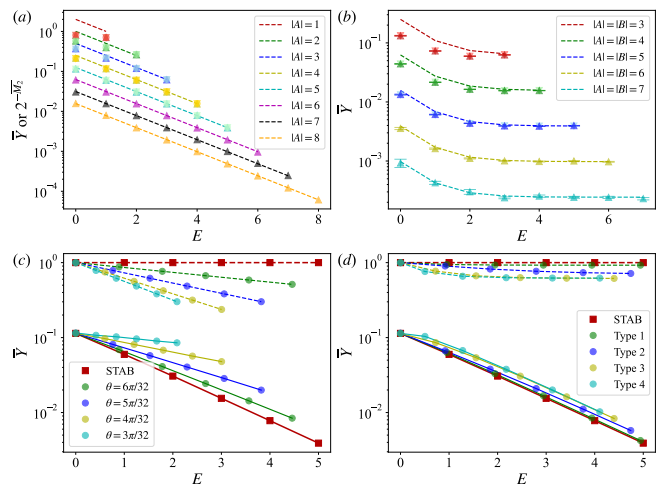


FIG. 2. (a) Numerical simulations of the setup depicted in Fig. 1(a). We consider initial states of the form Eq. (2) with varying $|A|$ and E . We compute the average value of \bar{Y} (upper triangles), as well as $2^{-\bar{M}_2}$ (lower triangles), where \bar{M}_2 is the average value of the second stabilizer Rényi entropy. The analytical result Eq. (1) is shown as dashed lines. (b) Numerical simulations of the setup depicted in Fig. 1(b). Choice of the initial state is the same as in (a). The analytic result Eq. (4) is shown as dashed lines. (c) Same as in (a) but for non-stabilizer initial states with k imperfect Bell pairs $|\phi_\theta\rangle = \cos\theta|00\rangle + \sin\theta|11\rangle$ shared between A and B . We compute the magic already existing in the initial state \bar{Y}_{ini} (dashed lines) and the change after the action of U_A : $\bar{Y}_{\text{final}}/\bar{Y}_{\text{ini}}$ (solid lines). (d) Same as in (c) but initial states are now constructed with four different types of entanglement spectra (see main text). Error bars are smaller than the size of the data points and hence not visible.

$U_B^{\text{Cliff}}|\psi\rangle$ such that

$$|\Phi\rangle = |+\rangle^{\otimes f_A} |\text{Bell}\rangle_{AB}^{\otimes E} |+\rangle^{\otimes f_B}, \quad (2)$$

which is illustrated in Fig. 1(d). The state consists of f_A and f_B qubits in $|+\rangle$ state in subsystem A and B , respectively, along with E Bell pairs shared between A and B , so that the entanglement entropy between A and B is E . Since \bar{Y} is obtained by averaging over the Haar random ensemble, U_A^{Cliff} can be simply absorbed into the average. Moreover, $Y(\rho)$ is invariant under Clifford unitary U_B^{Cliff} . Thus we have

$$\mathbb{E}_{U_A} Y \left(U_A |\psi\rangle\langle\psi| U_A^\dagger \right) = \mathbb{E}_{U_A} Y \left(U_A |\Phi\rangle\langle\Phi| U_A^\dagger \right) \quad (3)$$

for an arbitrary stabilizer state $|\psi\rangle$. We numerically average over $Y(U_A|\Phi\rangle\langle\Phi|U_A^\dagger)$ with Haar random U_A for various values of $|A|$ and E . The results are shown in Fig. 2(a), where we find excellent agreement with the analytical prediction of Eq. (1). In particular, the subleading corrections become negligible already at moderate subsystem sizes and entanglement $|A| + E \gtrsim 4$. We also simulate the Haar averaged second stabilizer Rényi entropy \bar{M}_2 , which turns out to be extremely close to

$\log \bar{Y}$. This implies that the average in Eq. (1) is also typical, as sample-to-sample fluctuations are extremely small. The same qualitative behavior holds if U_A is given by a brickwork circuit instead of Haar random unitary, but the total injected magic is limited by the depth (see SM [41]).

One can further explore the most general approach to magic injection while preserving the entanglement spectrum. Starting from a stabilizer state, we now apply a unitary that is a tensor product of local unitaries acting on subsystems A and B : $U = U_A \otimes U_B$, as illustrated in Fig. 1(b). We compute the linear stabilizer entropy of the resulting state, averaged over Haar random U_A and U_B . In the limit where $|A| \gg 1$ and $|B| \gg 1$, we find [41]

$$\begin{aligned} \bar{Y} &= \mathbb{E}_{U_A} \mathbb{E}_{U_B} Y \left(U_A U_B |\psi\rangle \langle \psi| U_A^\dagger U_B^\dagger \right) \\ &= 4 \cdot 2^{-N} \left[1 + 3 \cdot 2^{-2E} + O(2^{-|A|-E}) + O(2^{-|B|-E}) \right], \end{aligned} \quad (4)$$

where $N = |A| + |B|$ is the total number of qubits. This result reveals an intriguing mechanism by which stabilizer entanglement facilitates magic saturation. Notice that the average value of \bar{Y} for Haar random states is given by $4 \cdot 2^{-N}$. Eq. (4) shows that the gap between \bar{Y} for a stabilizer state acted upon by $U_A \otimes U_B$ and that for a Haar random state decays exponentially with the amount of entanglement. In other words, despite the applied unitary being a tensor product of local unitaries on subsystems A and B , from the perspective of magic, its effect on magic injection closely resembles that of a genuinely global Haar-random unitary, provided that the initial state is sufficiently entangled. Interestingly, the amount of entanglement necessary for such indistinguishability from Haar random magic is independent of system size. In Fig. 2(b), we numerically simulate this set up using the initial state (2) and averaging over Haar random unitaries U_A and U_B . Again, we find excellent agreement with the prediction of Eq. (4), with the subleading corrections negligible for moderate subsystem sizes and entanglement. Moreover, the average \bar{Y} saturates to that of a Haar random state already at $E \approx 3$, which is independent of system size.

Tripartite entanglement.- The above results for bipartite systems can be naturally extended to tripartite systems. Consider a stabilizer state shared among three parties A , B and C . Since any tripartite stabilizer state can be transformed via local unitaries acting on A , B , and C into a collection of GHZ state, Bell pair states, and single-qubit states [43], we can, without loss of generality, consider initial states as depicted in Fig. 1(e). Specifically, the initial state consists of g GHZ states shared among A , B , and C ; b_{AB} , b_{AC} , and b_{BC} Bell pairs shared between subsystems AB , AC , and BC , respectively, and f_A , f_B , f_C single-qubit states in each individual subsystem. Since magic injection via unitary operations on any single subsystem in this setting mirrors the bipartite case discussed earlier, we first consider unitaries of the form

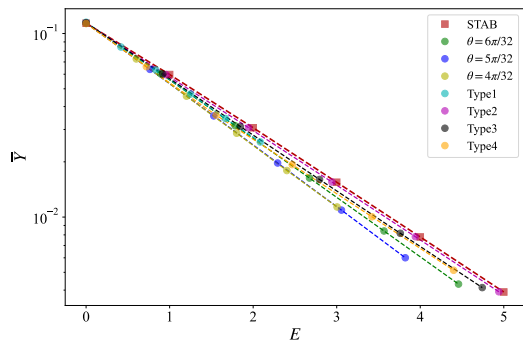


FIG. 3. Same as in Fig. 2(c)&(d), but now plotting \bar{Y}_{final} in each case considered.

$U = U_A \otimes U_B$ [Fig. 1(c)]. In the limit where $|A| \gg 1$ and $|B| \gg 1$, we find that the average \bar{Y} after applying U is given by [41]

$$\begin{aligned} \bar{Y} &= \mathbb{E}_{U_A} \mathbb{E}_{U_B} Y \left(U_A U_B |\psi\rangle \langle \psi| U_A^\dagger U_B^\dagger \right) \\ &= 4 \cdot 2^{-|A|-|B|-g-b_{AC}-b_{BC}} \left[1 + 3 \cdot 2^{-2b_{AB}-g} \right], \end{aligned} \quad (5)$$

where subleading corrections are of order $O(2^{-|A|}, 2^{-|B|})$. Eq. (5) can be understood as follows. The average value \bar{Y} is once again exponentially suppressed in both the total size of the subregion where the unitary is applied: $|A| + |B|$, and the amount of entanglement between subregion AB and its complement: $g + b_{AC} + b_{BC}$. Hence the physical interpretation of the prefactor in Eq. (5) is identical to that of Eq. (1). The discrepancy between these two cases lies in the additional factor $3 \cdot 2^{-2b_{AB}-g}$, which becomes negligible once A and B are sufficiently entangled. This is precisely what we have seen in Eq. (4): the effect of a factorized unitary $U_A \otimes U_B$ becomes essentially indistinguishable from that of a global unitary from the standpoint of magic, once A and B are sufficiently entangled. Thus, Eq. (5) encapsulates the combined effects of Eqs. (1) and (4) in the tripartite setting. In the SM [41], we further consider a factorized unitary acting on all three subregions: $U = U_A \otimes U_B \otimes U_C$, where we confirm that in this case the effect of a factorized Haar random unitary on magic injection again becomes indistinguishable from that of a global Haar random unitary, provided that the subregions are sufficiently entangled with one another.

Non-stabilizer entanglement.- So far, we have focused on the propagation of magic on stabilizer states. However, realistic dynamics almost always contains magic in the initial state. Does non-stabilizerness of this kind impose any road blocks on the magic highway? Our findings strongly suggest that, to leading order, the answer is no. Again consider an entangled initial state on AB where U_A is applied to inject magic. Since any initial magic local to A can be absorbed via the averaging of U_A , let us start with a state where non-stabilizerness only lives in the quantum correlation. Such a state is known to have non-local magic, which is non-trivial as

long as the entanglement spectrum is non-flat [28]. The simplest example of such a state consists of k imperfect Bell pairs shared between A and B : $|\psi\rangle = |0\rangle^{\otimes f_A} |\phi_\theta\rangle_{AB}^{\otimes k}$, where $|\phi_\theta\rangle = \cos\theta|00\rangle + \sin\theta|11\rangle$. Since k copies of $|\phi_\theta\rangle$ each with entanglement S can be unitarily distilled into $E = Sk - O(\sqrt{k})$ number of perfect Bell states tensoring a magic state on the $O(\sqrt{k})$ remaining qubits to good approximation [44], our previous analysis with stabilizer initial state again applies to leading order. That is, magic injection by U_A will increase in the same way as one increases the total entanglement E . Interestingly, this simple dependence also appears to extend to other states with non-local magic. For example, initial states with non-local magic can be parametrized in the form $|\psi\rangle = |0\rangle^{\otimes f_A} \sum_{i=1}^{2^k} \lambda_i |i\rangle_A \otimes |i\rangle_B$, where $|i\rangle$ denotes a computational basis state of k qubits. We choose four arbitrary entanglement spectra: (i) $\lambda_i \propto e^{-i/2^k}$; (ii) $\lambda_i \propto i$; (iii) $\lambda_i \propto i^2$; (iv) $\lambda_i \propto i^3$ and examine the magic spread numerically. Magic propagation is again displaying an E dependence similar to having a stabilizer state or imperfect Bell states as the initial state (Fig. 3).

Nonetheless, more care is needed going beyond leading order. It is clear that there is non-stabilizerness dependence even in the simplest example with imperfect Bell states at the order of $O(\sqrt{k})$. Furthermore, because initial states can contain magic, the remaining magic capacity for further injection is reduced, i.e., the change of total magic per magic state injection is smaller compared to stabilizer entanglement. We numerically calculate both the magic already existing in the initial states \bar{Y}_{ini} and the change after the action of U_A : $\bar{Y}_{\text{final}}/\bar{Y}_{\text{ini}}$. As shown in Fig. 2(c,d), \bar{Y}_{ini} itself in general decays with the increase of entanglement. Nonetheless, we find that the ratio $\bar{Y}_{\text{final}}/\bar{Y}_{\text{ini}}$ also decays exponentially with the amount of entanglement. For the same E , the change in

global magic becomes smaller as the initial state becomes more magical.

Discussion.- In this work, we demonstrate that stabilizer entanglement functions as a highway that facilitates the spread of locally injected magic throughout the entire system. In particular, we consider an analytically tractable setup where a local Haar random unitary acts on a subregion of a non-magical but potentially highly entangled state, thereby separating the process of magic injection from entanglement generation. We find that the average magic, as quantified by the linear stabilizer entropy, is enhanced by stabilizer entanglement. We further generalize our results to tripartite entanglement and non-stabilizer entanglement. A few interesting open questions remain. Our results for imperfect Bell-pair states suggest that the average amount of injected magic decreases as the amount of magic already existing in the target state increases. This implies that there may be a notion of intrinsic magic capacity of a given state that depends on both its entanglement and magic. Addressing this question would require a more systematic extension of our results to non-stabilizer states, which we leave for future work. Secondly, once we replace the Haar random U_A with a more structured brickwork circuit, the question of what is the minimal circuit depth required for the effect of magic injection to coincide with that of a Haar random U_A is worth exploring. The question is perhaps intimately related to the complexity growth of local random unitary circuits with circuit depth.

Acknowledgement.- We thank Cheng Wang, Yingfei Gu, and Yuzhen Zhang for helpful discussions. This work is supported by Grant No. 12375027 from the National Natural Science Foundation of China (Z.-C. Y.). Numerical simulations were performed on the High-performance Computing Platform of Peking University.

-
- [1] A. Hamma, R. Ionicioiu, and P. Zanardi, Ground state entanglement and geometric entropy in the Kitaev model, *Physics Letters A* **337**, 22–28 (2005).
 - [2] M. Levin and X.-G. Wen, Detecting topological order in a ground state wave function, *Physical Review Letters* **96**, 10.1103/physrevlett.96.110405 (2006).
 - [3] A. Kitaev and J. Preskill, Topological entanglement entropy, *Phys. Rev. Lett.* **96**, 110404 (2006).
 - [4] B. Skinner, J. Ruhman, and A. Nahum, Measurement-induced phase transitions in the dynamics of entanglement, *Physical Review X* **9**, 10.1103/physrevx.9.031009 (2019).
 - [5] S. Ryu and T. Takayanagi, Holographic derivation of entanglement entropy from the anti-de Sitter space/conformal field theory correspondence, *Physical Review Letters* **96**, 10.1103/physrevlett.96.181602 (2006).
 - [6] D. Gottesman, The Heisenberg representation of quantum computers, arXiv preprint quant-ph/9807006 (1998).
 - [7] S. Aaronson and D. Gottesman, Improved simulation of stabilizer circuits, *Physical Review A* **70**, 10.1103/physreva.70.052328 (2004).
 - [8] M. Howard and E. Campbell, Application of a resource theory for magic states to fault-tolerant quantum computing, *Phys. Rev. Lett.* **118**, 090501 (2017).
 - [9] V. Veitch, S. A. Hamed Mousavian, D. Gottesman, and J. Emerson, The resource theory of stabilizer quantum computation, *New Journal of Physics* **16**, 013009 (2014).
 - [10] M. Heinrich and D. Gross, Robustness of magic and symmetries of the stabiliser polytope, *Quantum* **3**, 132 (2019).
 - [11] H. Pashayan, J. J. Wallman, and S. D. Bartlett, Estimating outcome probabilities of quantum circuits using quasiprobabilities, *Phys. Rev. Lett.* **115**, 070501 (2015).
 - [12] M. Howard, J. Wallman, V. Veitch, and J. Emerson, Contextuality supplies the ‘magic’ for quantum computation, *Nature* **510**, 351–355 (2014).
 - [13] S. Bravyi and A. Kitaev, Universal quantum computation with ideal Clifford gates and noisy ancillas, *Physical Review A* **71**, 10.1103/physreva.71.022316 (2005).
 - [14] S. Bravyi and J. Haah, Magic-state distillation with

- low overhead, *Physical Review A* **86**, [10.1103/physreva.86.052329](https://doi.org/10.1103/physreva.86.052329) (2012).
- [15] S. Sarkar, C. Mukhopadhyay, and A. Bayat, Characterization of an operational quantum resource in a critical many-body system, *New Journal of Physics* **22**, 083077 (2020).
- [16] C. D. White and J. H. Wilson, Mana in haar-random states, arXiv preprint arXiv:2011.13937 (2020).
- [17] C. D. White, C. Cao, and B. Swingle, Conformal field theories are magical, *Phys. Rev. B* **103**, 075145 (2021), [arXiv:2007.01303 \[quant-ph\]](https://arxiv.org/abs/2007.01303).
- [18] Z.-W. Liu and A. Winter, Many-body quantum magic, *PRX Quantum* **3**, [10.1103/prxquantum.3.020333](https://doi.org/10.1103/prxquantum.3.020333) (2022).
- [19] P. Niroula, C. D. White, Q. Wang, S. Johri, D. Zhu, C. Monroe, C. Noel, and M. J. Gullans, Phase transition in magic with random quantum circuits, *Nature Phys.* **20**, 1786 (2024), [arXiv:2304.10481 \[quant-ph\]](https://arxiv.org/abs/2304.10481).
- [20] A. Catalano, J. Odavić, G. Torre, A. Hamma, F. Franchini, and S. Giampaolo, Magic phase transition and non-local complexity in generalized w state, arXiv preprint arXiv:2406.19457 (2024).
- [21] S. Zhou, Z.-C. Yang, A. Hamma, and C. Chamon, Single t gate in a clifford circuit drives transition to universal entanglement spectrum statistics, *SciPost Physics* **9**, 087 (2020).
- [22] T. J. Sewell and C. D. White, Mana and thermalization: Probing the feasibility of near-clifford hamiltonian simulation, *Phys. Rev. B* **106**, 125130 (2022).
- [23] D. Rattacaso, L. Leone, S. F. E. Oliviero, and A. Hamma, Stabilizer entropy dynamics after a quantum quench, *Phys. Rev. A* **108**, 042407 (2023).
- [24] Y. Zhang and Y. Gu, Quantum magic dynamics in random circuits, arXiv preprint arXiv:2410.21128 (2024).
- [25] G. E. Fux, B. Béri, R. Fazio, and E. Tirrito, Disentangling unitary dynamics with classically simulable quantum circuits, arXiv preprint arXiv:2410.09001 (2024).
- [26] C. Fan, X. Qian, H.-C. Zhang, R.-Z. Huang, M. Qin, and T. Xiang, Disentangling critical quantum spin chains with clifford circuits, *Phys. Rev. B* **111**, 085121 (2025).
- [27] C. Cao, Non-trivial area operators require non-local magic, *JHEP* **11**, 105, [arXiv:2306.14996 \[hep-th\]](https://arxiv.org/abs/2306.14996).
- [28] C. Cao, G. Cheng, A. Hamma, L. Leone, W. Munizzi, and S. F. Oliviero, Gravitational back-reaction is magical, arXiv preprint arXiv:2403.07056 (2024).
- [29] E. Tirrito, P. S. Tarabunga, G. Lami, T. Chanda, L. Leone, S. F. E. Oliviero, M. Dalmonte, M. Collura, and A. Hamma, Quantifying nonstabilizerness through entanglement spectrum flatness, *Phys. Rev. A* **109**, L040401 (2024).
- [30] M. Viscardi, M. Dalmonte, A. Hamma, and E. Tirrito, **Interplay of entanglement structures and stabilizer entropy in spin models** (2025), [arXiv:2503.08620 \[quant-ph\]](https://arxiv.org/abs/2503.08620).
- [31] D. Iannotti, G. Esposito, L. C. Venuti, and A. Hamma, **Entanglement and stabilizer entropies of random bipartite pure quantum states** (2025), [arXiv:2501.19261 \[quant-ph\]](https://arxiv.org/abs/2501.19261).
- [32] J. Huang, X. Qian, and M. Qin, **Non-stabilizerness entanglement entropy: a measure of hardness in the classical simulation of quantum many-body systems** (2024), [arXiv:2409.16895 \[quant-ph\]](https://arxiv.org/abs/2409.16895).
- [33] X. Turkeshi, E. Tirrito, and P. Sierant, Magic spreading in random quantum circuits, arXiv preprint arXiv:2407.03929 (2024).
- [34] E. Tirrito, X. Turkeshi, and P. Sierant, Anticoncentration and magic spreading under ergodic quantum dynamics, arXiv preprint arXiv:2412.10229 (2024).
- [35] N. Bao, C. Cao, and V. P. Su, Magic state distillation from entangled states, *Physical Review A* **105**, [10.1103/physreva.105.022602](https://doi.org/10.1103/physreva.105.022602) (2022).
- [36] F. Wei and Z.-W. Liu, Noise robustness and threshold of many-body quantum magic, arXiv preprint arXiv:2410.21215 (2024).
- [37] J. Odavić, M. Viscardi, and A. Hamma, Stabilizer entropy in non-integrable quantum evolutions, arXiv preprint arXiv:2412.10228 (2024).
- [38] L. Leone and L. Bittel, Stabilizer entropies are monotones for magic-state resource theory, *Phys. Rev. A* **110**, L040403 (2024).
- [39] L. Leone, S. F. E. Oliviero, and A. Hamma, Stabilizer rényi entropy, *Phys. Rev. Lett.* **128**, 050402 (2022).
- [40] T. Metger, A. Poremba, M. Sinha, and H. Yuen, Simple Constructions of Linear-Depth t-Designs and Pseudorandom Unitaries, in [2024 IEEE 65th Annual Symposium on FOCS](https://doi.org/10.1109/FOCS52357.2024) (IEEE Computer Society, Los Alamitos, CA, USA, 2024) pp. 485–492.
- [41] See Supplemental Material.
- [42] D. Fattal, T. S. Cubitt, Y. Yamamoto, S. Bravyi, and I. L. Chuang, Entanglement in the stabilizer formalism, arXiv preprint quant-ph/0406168 (2004).
- [43] S. Bravyi, D. Fattal, and D. Gottesman, Ghz extraction yield for multipartite stabilizer states, *Journal of Mathematical Physics* **47** (2006).
- [44] H.-K. Lo and S. Popescu, Classical communication cost of entanglement manipulation: Is entanglement an interconvertible resource?, *Phys. Rev. Lett.* **83**, 1459 (1999).
- [45] P. W. Brouwer and C. W. J. Beenakker, Diagrammatic method of integration over the unitary group, with applications to quantum transport in mesoscopic systems, *Journal of Mathematical Physics* **37**, 4904–4934 (1996).
- [46] S. Samuel, $U(n)$ integrals, $1/n$, and the de Wit–t hooft anomalies, *Journal of Mathematical Physics* **21**, 2695 (1980), https://pubs.aip.org/aip/jmp/article-pdf/21/12/2695/19003229/2695_1_online.pdf.

Supplemental Material for “Stabilizer entanglement as a magic highway”

Appendix A: Analytical method

In this section, we present the analytical method used to derive the main results quoted in the main text. In Section A 1, we provide a brief introduction to a diagrammatic approach for computing polynomials of matrix elements of unitary matrices averaged over the Haar ensemble. Section A 2 introduces a key quantity used throughout our analysis and outlines approximations made to simplify both the calculation and the final results. Finally, in Section A 3, we detail the step-by-step derivation of the results presented in the main text.

1. A diagrammatic approach

In this subsection, we outline a diagrammatic method for systematically computing expectation values of polynomials in the matrix elements of unitary matrices under the Haar ensemble. Our presentation closely follows the original work of Brouwer (1996) [45]. Consider a polynomial function of the form

$$f(U) = U_{a_1 b_1} \dots U_{a_n b_n} U_{\alpha_1 \beta_1}^* \dots U_{\alpha_m \beta_m}^* \quad (\text{A1})$$

where U_{ij} and U_{kl}^* denote matrix elements of a unitary matrix and its complex conjugate, respectively. The Haar measure expectation value of such functions, denoted by $\overline{f(U)} := \mathbb{E}_{\text{Haar}}[f(U)]$, is given by

$$\overline{f(U)} = \delta_{nm} \sum_{P, P'} V_{P, P'} \prod_{j=1}^n \delta_{a_j \alpha_{P(j)}} \delta_{b_j \beta_{P'(j)}} \quad (\text{A2})$$

where the summation is over all permutations P and P' of the integers $(1, \dots, n)$. The coefficients $V_{P, P'}$ depend only on the cycle structure of the permutation $P^{-1}P'$ [46]. In other words, it only depends on the lengths c_1, \dots, c_k of the cycles in the factorization of $P^{-1}P'$. So below we write V_{c_1, \dots, c_k} instead of $V_{P, P'}$.

The diagrams consist of the building blocks shown in Fig. 4. The matrix elements U_{ab} or $U_{\alpha\beta}^*$ are represented by thick dotted lines. The first index (a or α) is represented by a black dot, the second index (b or β) is represented by a white dot. Matrix element A_{ij} of a fixed matrix A (i.e., a matrix that is not part of the average) is represented by a directed thick solid line, pointing from the first to the second index, without dots at the endpoints. The Kronecker delta is represented by an undirected thin solid line, without dots at the endpoints. Two dots connected by a solid line indicate contractions of their corresponding matrix indices. As an example, the functions $f(U) = \text{Tr}(AUBU^\dagger)$ and $g(U) = \text{Tr}(AUBUCU^\dagger DU^\dagger)$ are represented in Fig. 5.

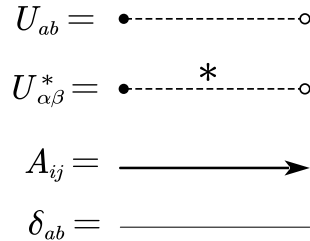


FIG. 4. Diagrammatic representations for the unitary matrix U and U^* , the fixed matrix A and the Kronecker delta.

Since the average over Haar random ensemble leads to a summation of permutations, we need to keep track of each term in the summation in Eq. (A2) by keeping track of P and P' in the diagram. Each P represents one way of pairing the first index of U with that of U^* , and P' pairs the second index of U with that of U^* . This pairing is represented by adding additional thin lines connecting the endpoints of U and that of U^* in the diagram, with black dots connected to black dots, and white dots connected to white dots, as depicted in Fig. 5. To associate each diagram with a specific value, we follow the following rules:

- (i) Cycle structure: A closed circuit consisting of alternating dotted or thin lines correspond to a cycle in $P^{-1}P'$. The length c_k of it is half the number of dotted lines in the circuit. We call the circuit a U -cycle of length c_k .
- (ii) Matrix trace: A closed circuit consisting of alternating thick or thin lines is called a T -cycle. A T -cycle containing matrices $A^{(1)}, A^{(2)}, \dots, A^{(k)}$ (ordered when going in one direction of the closed circuit) corresponds to

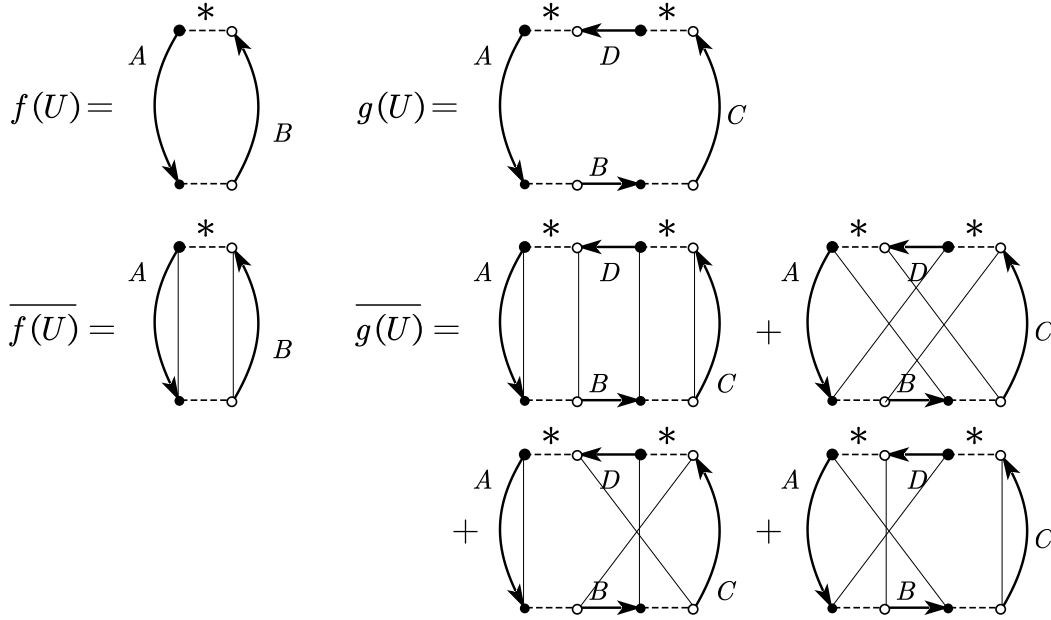


FIG. 5. Top: diagrams representing $f(U) = \text{Tr}(AUBU^\dagger)$ and $g(U) = \text{Tr}(AUBUCU^\dagger DU^\dagger)$, respectively. Bottom: diagrams that keep track of all terms after taking the average over Haar random U . The average of $\overline{f(U)}$ contains only one term, whereas $\overline{g(U)}$ contains four terms.

$\text{Tr}A^{(1)}A^{(2)}\dots A^{(k)}$ (recall that thin lines represent δ_{ab} that locks the two indices they connect). If a thick line corresponding to matrix A is traversed in the opposite direction, the matrix is replaced by its transpose A^T .

To illustrate this procedure, we consider the averages of the functions $f(U) = \text{Tr}(AUBU^\dagger)$ and $g(U) = \text{Tr}(AUBUCU^\dagger DU^\dagger)$. By connecting the dots with thin lines, we obtain the diagrams shown in Fig. 5. For f , there is only one diagram, which consists of a single U -cycle of length 1 (with weight V_1) and two T -cycles, which generate $\text{Tr}A$ and $\text{Tr}B$. Thus, the expected value is:

$$\overline{f(U)} = V_1 \text{Tr}A \text{Tr}B. \quad (\text{A3})$$

As for g , there are four diagrams that contribute. The first diagram contains two U -cycles of length 1, and three T -cycles. Its contribution is $V_{1,1} \text{Tr}A \text{Tr}(BD) \text{Tr}C$. The second diagram contains two U -cycles of length 1 and a single T -cycle. Its contribution is $V_{1,1} \text{Tr}(ABCD)$. The third and fourth diagram each contain a single U -cycle of length 2 and two T -cycles. Their contributions are $V_2 \text{Tr}A \text{Tr}(BDC)$ and $V_2 \text{Tr}(ADB) \text{Tr}C$. So we obtain:

$$\overline{g(U)} = V_{1,1} [\text{Tr}(ABCD) + \text{Tr}A \text{Tr}(BD) \text{Tr}C] + V_2 [\text{Tr}A \text{Tr}(BDC) + \text{Tr}(ADB) \text{Tr}C]. \quad (\text{A4})$$

2. A useful quantity and its approximations

In this subsection, we define a quantity that will be used intensively in evaluating \overline{Y} . We will calculate the value of this quantity in its most general form, to leading order in $2^{|A|+E}$, where E is the entanglement entropy. Let \mathbb{S}_A denote an $|A|$ -qubit stabilizer group whose size is 2^{f_A} with $f_A < |A|$; then let $u_i, i = 1, 2, 3, 4$ denote four Pauli strings supported on A (where some of them can be identical) that commute with every element in \mathbb{S}_A (i.e. u_i is in the normalizer group of \mathbb{S}_A). Notice that we allow $u_i = I_A$, but otherwise $u_i \notin \mathbb{S}_A$. Since we assume $f_A < |A|$, one can always find a nontrivial u_i . And because $u_i \mathbb{S}_A = u_i g \mathbb{S}_A, \forall g \in \mathbb{S}_A$, we can choose one specific u_i . Then we define the following function:

$$\alpha_{P_A}(u_1, u_2, u_3, u_4) := \overline{\prod_{i=1}^4 \text{Tr}(P_A U_A u_i \mathbb{S}_A U_A^\dagger)}, \quad (\text{A5})$$

where P_A is a Pauli string supported on subsystem A . In the above definition, we also abuse notation by using \mathbb{S}_A to represent an equal weight summation of all elements in \mathbb{S}_A : $\sum_{g \in \mathbb{S}_A} g$. The connection between the above quantity

and \bar{Y} will be explained in detail in the next subsection. Basically it naturally arises when computing $\text{Tr}(PU_A\rho U_A^\dagger)^4$, with ρ represented as a projector onto the stabilizer subspace.

Eq. (A5) can be represented using the diagrammatic method introduced in Sec. A1 as follows:

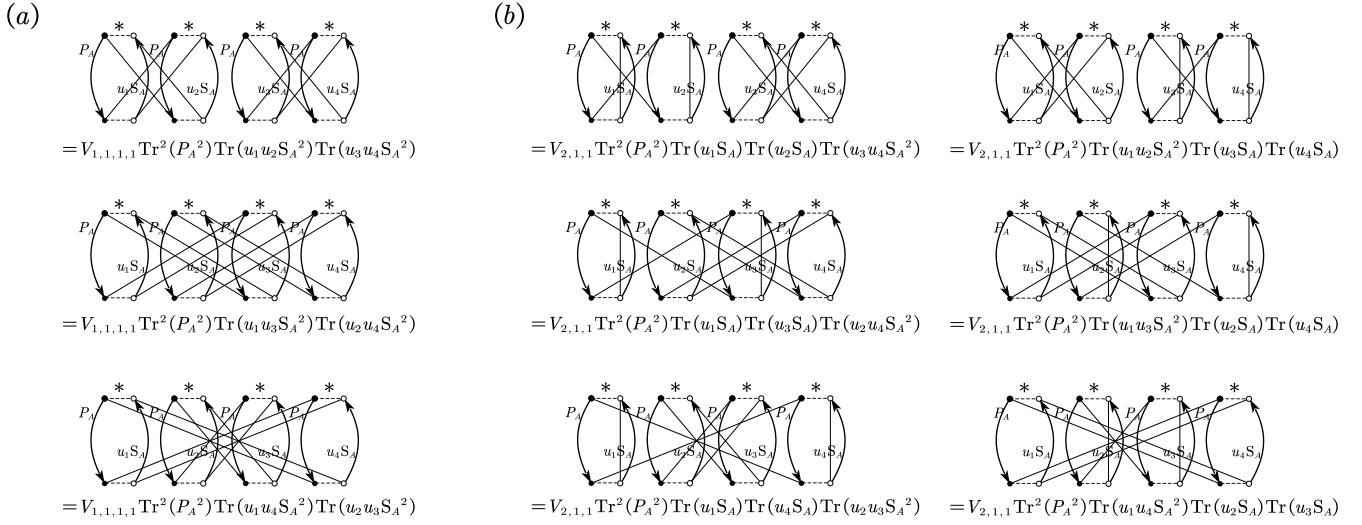


FIG. 6. (a) Leading order and the corresponding diagrams for $\alpha_{P_A}(u_1, u_2, u_3, u_4)$. There are $4!^2 = 576$ diagrams in total. If $P_A \neq I_A$, then $\text{Tr}(P_A) = \text{Tr}(P_A^3) = 0$, and there are 216 diagrams with non-zero contributions. (b) Subleading order and the corresponding diagrams for $\alpha_{P_A}(u_1, u_2, u_3, u_4)$.

First of all, the factors $V_{c_1, c_2, \dots}$ can be readily obtained using known results of Weingarten functions. Let $N := 2^{|A|}$, we have:

$$\begin{aligned} V_{1,1,1,1} &= \frac{N^4 - 8N^2 + 6}{N^2(N^2 - 1)(N^2 - 4)(N^2 - 9)} = 2^{-4|A|} + 6 \cdot 2^{-6|A|} + O(2^{-8|A|}), \\ V_{2,1,1} &= \frac{-N^3 + 4N}{N^2(N^2 - 1)(N^2 - 4)(N^2 - 9)} = -2^{-5|A|} + 18 \cdot 2^{-7|A|} + O(2^{-9|A|}), \\ V_{2,2} &= \frac{N^2 + 6}{N^2(N^2 - 1)(N^2 - 4)(N^2 - 9)} = 2^{-6|A|} + 20 \cdot 2^{-8|A|} + O(2^{-10|A|}), \\ V_{3,1} &= \frac{2N^2 - 6}{N^2(N^2 - 1)(N^2 - 4)(N^2 - 9)} = 2 \cdot 2^{-6|A|} + 8 \cdot 2^{-8|A|} + O(2^{-10|A|}), \\ V_4 &= \frac{-5N}{N^2(N^2 - 1)(N^2 - 4)(N^2 - 9)} = -5 \cdot 2^{-7|A|} + O(2^{-9|A|}). \end{aligned} \quad (\text{A6})$$

Careful inspections of all diagrams reveals that factors involving P_A are of the form $\text{Tr}^4(P_A)$, $\text{Tr}(P_A^3)\text{Tr}(P_A)$, $\text{Tr}(P_A^2)\text{Tr}^2(P_A)$, $\text{Tr}^2(P_A^2)$, and $\text{Tr}(P_A^4)$. Notice that $P_A^2 = P_A^4 = I_A$, $P_A^3 = P_A$. Also, if $P_A \neq I_A$, $\text{Tr}(P_A) = 0$. Thus, in this case, the only non-zero contributions come from terms involving $\text{Tr}^2(P_A^2) = 2^{2|A|}$ and $\text{Tr}(P_A^4) = 2^{|A|}$. Similarly, terms involving u_i and S_A are of the form $\text{Tr}(u_1 u_2 u_3 u_4 S_A^4)$, $\text{Tr}(u_1 u_2 u_3 S_A^3)\text{Tr}(u_4 S_A)$, $\text{Tr}(u_1 u_2 S_A^2)\text{Tr}(u_3 u_4 S_A^2)$, $\text{Tr}(u_1 u_2 S_A^2)\text{Tr}(u_3 S_A)\text{Tr}(u_4 S_A)$, and $\text{Tr}(u_1 S_A)\text{Tr}(u_2 S_A)\text{Tr}(u_3 S_A)\text{Tr}(u_4 S_A)$ (and also permutations of the u_i 's). It is also useful to remember $\text{Tr}(S_A) = 2^{|A|}$, and $\text{Tr}(S_A^2) = 2^{|A|+f_A}$.

When $P_A = I_A$, α_{I_A} trivially becomes $\prod_{i=1}^4 \text{Tr}(u_i S_A)$, which vanishes unless $u_i = I_A$, $\forall i$. We thus have:

$$\alpha_{I_A}(u_1, u_2, u_3, u_4) = 2^{4|A|} \delta_1(u_1) \delta_1(u_2) \delta_1(u_3) \delta_1(u_4), \quad (\text{A7})$$

where $\delta_1(u_i) = 1$ iff $u_i = I_A$ and zero otherwise.

When $P_A \neq I_A$, by carefully examining the structures of all diagrams, we find that the leading order contributions

to α_{P_A} come from the diagrams shown in Fig. 6.

$$\begin{aligned}
& \alpha_{P_A}(u_1, u_2, u_3, u_4) \\
&= 2^{2f_A} \left(\underbrace{\delta_2(u_1, u_2)\delta_2(u_3, u_4) + \text{permutations}}_{3 \text{ terms}} \right) \\
&\quad - 2^{f_A} \left(\underbrace{\delta_2(u_1, u_2)\delta_1(u_3)\delta_1(u_4) + \text{permutations}}_{6 \text{ terms}} \right) \\
&\quad + O\left(2^{3f_A-2|A|}\delta_4(u_1, u_2, u_3, u_4)\right),
\end{aligned} \tag{A8}$$

where $\delta_2(u_1, u_2) = 1$ iff $u_1 = u_2$, and zero otherwise; $\delta_4(u_1, u_2, u_3, u_4) = \frac{\text{Tr}(u_1 u_2 u_3 u_4)}{2^{|A|}}$. In the above equation, the first line comes from terms like $V_{1,1,1,1}\text{Tr}^2(P_A^2)\text{Tr}(u_1 u_2 S_A^2)\text{Tr}(u_3 u_4 S_A^2)$, and the 2nd line comes from $V_{2,1,1}\text{Tr}^2(P_A^2)\text{Tr}(u_1 u_2 S_A^2)\text{Tr}(u_3 S_A)\text{Tr}(u_4 S_A)$.

3. Derivation of the key results presented in the main text

In this subsection, we provide a detailed derivation of Eqs. (1), (4) and (5) in the main text.

a. Eq. (1)

We start with Eq. (1). The key to our derivation is to represent the initial state as a projector onto the stabilizer subspace, and a decomposition of the stabilizer group of the full system in terms of the cosets of stabilizer subgroups of subsystems A and B . Let \mathbb{S}_{AB} denote the stabilizer group of the initial state. Then initial density matrix can be written as a projector

$$\rho_0 = \frac{1}{2^N} \sum_{g \in \mathbb{S}_{AB}} g. \tag{A9}$$

Let \mathbb{S}_A and \mathbb{S}_B denote the stabilizer subgroups of subsystem A and B , respectively. Let E denote the entanglement entropy between subsystem A and B . We have $E = |A| - \dim(\mathbb{S}_A) = |B| - \dim(\mathbb{S}_B)$. \mathbb{S}_{AB} can then be decomposed in terms of the cosets of \mathbb{S}_A and \mathbb{S}_B as follows:

$$\mathbb{S}_{AB} = \underbrace{\mathbb{S}_A \otimes \mathbb{S}_B \cup a_1 \mathbb{S}_A \otimes b_1 \mathbb{S}_B \cup a_2 \mathbb{S}_A \otimes b_2 \mathbb{S}_B \cup \dots}_{4^E \text{ terms}} \tag{A10}$$

where $a_i \notin \mathbb{S}_A$ and $b_i \notin \mathbb{S}_B$ are the logical operators of subsystems A and B , respectively. To ensure the proper commutation relation, the logical operators must be paired up into (a_i, b_i) such that: (i) if $[a_i, a_j] = 0$, then $[b_i, b_j] = 0$; or (ii) if $\{a_i, a_j\} = 0$, then $\{b_i, b_j\} = 0$. While it is not hard to convince oneself that the above decomposition is correct for pure states with $\dim(\mathbb{S}_{AB}) = N$, let us check that the dimensions work out. First of all, since the entanglement between A and B is E , there are precisely E logical qubits encoded in both subsystems, with 4^E logical operators in each subsystem, and hence 4^E terms in the decomposition. Secondly, we can count the total number of group elements in \mathbb{S}_{AB} from the right-hand side of the decomposition. We have $4^E \times 2^{\dim(\mathbb{S}_A)} \times 2^{\dim(\mathbb{S}_B)} = 2^{|A|+|B|} = 2^N$, as it should. We will give a concrete example of such a decomposition in Appendix B.

We can now express the initial state using the above coset decomposition of \mathbb{S}_{AB} :

$$\rho_0 = \frac{1}{2^N} \mathbb{S}_{AB} = \frac{1}{2^N} \left(\underbrace{\mathbb{S}_A \otimes \mathbb{S}_B + a_1 \mathbb{S}_A \otimes b_1 \mathbb{S}_B + a_2 \mathbb{S}_A \otimes b_2 \mathbb{S}_B + \dots}_{4^E \text{ terms}} \right) \tag{A11}$$

Armed with the above representation of ρ_0 , we can cast the average value \bar{Y} as:

$$\begin{aligned}
\bar{Y} &= \frac{1}{2^{5N}} \sum_{P \in P_N} \overline{\text{Tr}^4(P U_A \mathbb{S}_{AB} U_A^\dagger)} \\
&= \frac{1}{2^{5N}} \sum_{P \in P_N} \sum_{k=0}^{2^{2E}-1} \alpha_{P_A}(a_k, a_k, a_k, a_k) \text{Tr}^4(P_B b_k \mathbb{S}_B).
\end{aligned} \tag{A12}$$

In going from the first to the second line, notice that the Pauli string $P = P_A \otimes P_B$, and that the unitary U_A is supported on subsystem A and hence leaves P_B invariant. Moreover, since different cosets $b_j \mathcal{S}_B$ do not overlap, for a given P (and P_B), there is at most one coset such that $\text{Tr}^4(P_B b_k \mathcal{S}_B)$ does not vanish. The trace involving P_A is now exactly of the form in Eq. (A5), with $u_1 = u_2 = u_3 = u_4 = a_k$ for some k . We can now directly apply our general results in Eqs. (A7) and (A8).

Consider first a fixed Pauli string P and k , which corresponds to one term of the summation in \bar{Y} . We have the following result:

$$\begin{aligned} & \alpha_{P_A}(a_k, a_k, a_k, a_k) \text{Tr}^4(P_B b_k \mathcal{S}_B) \\ = & \delta(P_B, b_k \mathcal{S}_B) \times \begin{cases} 3 \cdot 2^{2|A|+4|B|-2E} [1 - 2 \cdot 2^{E-|A|} + O(2^{-E-|A|})], & P_A \neq I_A, \quad k = 0 \\ 3 \cdot 2^{2|A|+4|B|-2E} [1 + O(2^{-E-|A|})], & P_A \neq I_A, \quad k \neq 0 \\ 2^{4|A|+4|B|}, & P_A = I_A, \quad k = 0 \\ 0, & P_A = I_A, \quad k \neq 0 \end{cases} \end{aligned} \quad (\text{A13})$$

In the above equation, $k = 0$ corresponds to the first term in the coset decomposition, with $a_0 = b_0 = I$; $\delta(P_B, b_k \mathcal{S}_B) = 1$ iff $P_B \in b_k \mathcal{S}_B$, and zero otherwise. Summing over $P \in P_N$ and k , we have:

$$\begin{aligned} & \sum_{P \in P_N} \sum_{k=0}^{2^{2E}-1} \alpha_{P_A}(a_k, a_k, a_k, a_k) \text{Tr}^4(P_B b_k \mathcal{S}_B) \\ = & \underbrace{2^{|B|-E} \cdot (2^{2|A|} - 1) \cdot 3 \cdot 2^{2|A|+4|B|-2E} [1 - 2 \cdot 2^{E-|A|} O(2^{-E-|A|})]}_{P_A \neq I_A, \quad k=0} \\ + & \underbrace{2^{|B|-E} \cdot (2^{2E} - 1) \cdot (2^{2|A|} - 1) \cdot 3 \cdot 2^{2|A|+4|B|-2E} [1 + O(2^{-E-|A|})]}_{P_A \neq I_A, \quad k \neq 0} \\ + & \underbrace{2^{|B|-E} \cdot 2^{4|A|+4|B|}}_{P_A = I_A, \quad k=0} \\ = & 4 \cdot 2^{4|A|+5|B|-E} [1 + O(2^{-|A|-E})]. \end{aligned} \quad (\text{A14})$$

In the above summation, the prefactor $(2^{2|A|} - 1)$ counts the total number of $P_A \neq I_A$; $(2^{|B|-E})$ comes from the size of each coset $|b_k \mathcal{S}_B|$. The final result is precisely Eq. (1) quoted in the main text after dividing by 2^{5N} .

b. Eq. (4)

We provide detailed calculations for Eq. (4) in the main text. Since the unitary acting on ρ_0 takes a factorized form $U = U_A \otimes U_B$, the average \bar{Y} similarly factorizes into

$$\bar{Y} = \frac{1}{2^{5N}} \sum_{P \in P_N} \sum_{k_1, k_2, k_3, k_4} \alpha_{P_A}(a_{k_1}, a_{k_2}, a_{k_3}, a_{k_4}) \beta_{P_B}(b_{k_1}, b_{k_2}, b_{k_3}, b_{k_4}), \quad (\text{A15})$$

where $\beta_{P_B}(b_{k_1}, b_{k_2}, b_{k_3}, b_{k_4})$ is defined analogously to Eq. (A5).

For convenience, we define the following functions:

$$f_1 := \underbrace{\delta_2(a_{k_1}, a_{k_2}) \delta_2(a_{k_3}, a_{k_4}) + \text{permutations}}_{3 \text{ terms}},$$

$$f_2 := \underbrace{\delta_2(a_{k_1}, a_{k_2}) \delta_1(a_{k_3}) \delta_1(a_{k_4}) + \text{permutations}}_{6 \text{ terms}},$$

$$f_3 := \delta_4(a_{k_1}, a_{k_2}, a_{k_3}, a_{k_4}),$$

where the definition of δ_2 and δ_4 was given below Eq. (A8). The above functions f_1, f_2 , and f_3 correspond to the three leading order contributions in $\alpha_{P_A \neq I_A}$ as given in Eq. (A8). We suppress the indices k_1, \dots, k_4 in the definition of f_i 's to simplify notation. We then have the following summations:

$$\sum_{k_1, k_2, k_3, k_4} f_1 = 3 \cdot 2^{4E}, \quad \sum_{k_1, k_2, k_3, k_4} f_2 = 6 \cdot 2^{2E}, \quad \sum_{k_1, k_2, k_3, k_4} f_3 \leq 2^{6E}.$$

Now, Eq. (A15) can be readily evaluated by summing over contributions from (i) $P_A \neq I_A, P_B \neq I_B$; (ii) $P_A \neq I_A, P_B = I_B$; (iii) $P_A = I_A, P_B \neq I_B$; (iv) $P_A = I_A, P_B = I_B$, using Eq. (A8). Let us consider contributions from each case.

(i) $P_A \neq I_A$ and $P_B \neq I_B$, we have:

$$\begin{aligned} & \sum_{k_1, k_2, k_3, k_4} \alpha_{P_A}(a_{k_1}, a_{k_2}, a_{k_3}, a_{k_4}) \beta_{P_B}(b_{k_1}, b_{k_2}, b_{k_3}, b_{k_4}) \\ &= 2^{2|A|+2|B|-4E} \sum_{k_1, k_2, k_3, k_4} f_1 f_1 - 2^{|A|+2|B|-3E} \sum_{k_1, k_2, k_3, k_4} f_1 f_2 + \\ & - 2^{2|A|+|B|-3E} \sum_{k_1, k_2, k_3, k_4} f_1 f_2 + 2^{|A|+|B|-2E} \sum_{k_1, k_2, k_3, k_4} f_2 f_2 + \\ & + c_1 \cdot 2^{|A|+2|B|-5E} \sum_{k_1, k_2, k_3, k_4} f_1 f_3 + c_1 \cdot 2^{2|A|+|B|-5E} \sum_{k_1, k_2, k_3, k_4} f_1 f_3 + \\ & + c_2 \cdot 2^{|A|+|B|-6E} \sum_{k_1, k_2, k_3, k_4} f_3 f_3 + c_3 \cdot 2^{|A|+|B|-4E} \sum_{k_1, k_2, k_3, k_4} f_2 f_3 \end{aligned} \quad (\text{A16})$$

We now analyze the order of magnitude of each term. Since $\sum_{k_1, k_2, k_3, k_4} f_i \cdot (\dots) \leq \sum_{k_1, k_2, k_3, k_4} f_i$, where (\dots) represents any product of δ_1, δ_2 , or δ_4 (as additional δ -functions further reduce the number of unconstrained summations over k_1, \dots, k_4), we have

$$\sum_{k_1, k_2, k_3, k_4} f_i^2 = \sum_{k_1, k_2, k_3, k_4} f_i + O(2^{-E}), \quad \sum_{k_1, k_2, k_3, k_4} f_i f_j \sim O(2^{-E}) \times \min(\sum f_i, \sum f_j). \quad (\text{A17})$$

A careful inspection of Eq. (A16) reveals that, in the limit $|A| \gg 1, |B| \gg 1$, the leading-order contribution comes from the term involving $\sum f_1^2$. We then have

$$\begin{aligned} & \sum_{k_1, k_2, k_3, k_4} \alpha_{P_A}(a_{k_1}, a_{k_2}, a_{k_3}, a_{k_4}) \beta_{P_B}(b_{k_1}, b_{k_2}, b_{k_3}, b_{k_4}) \\ &= 3 \cdot 2^{2|A|+2|B|} \left[1 + 2 \cdot 2^{-2E} + O(2^{-|A|-E}) + O(2^{-|B|-E}) \right]. \end{aligned} \quad (\text{A18})$$

(ii) $P_A = I_A$ and $P_B \neq I_B$. Recall $\alpha_{I_A}(a_{k_1}, a_{k_2}, a_{k_3}, a_{k_4}) = 2^{4|A|} \delta_1(a_{k_1}) \delta_1(a_{k_2}) \delta_1(a_{k_3}) \delta_1(a_{k_4})$. We have:

$$\begin{aligned} & \sum_{k_1, k_2, k_3, k_4} \alpha_{I_A}(a_{k_1}, a_{k_2}, a_{k_3}, a_{k_4}) \beta_{P_B}(b_{k_1}, b_{k_2}, b_{k_3}, b_{k_4}) \\ &= 3 \cdot 2^{4|A|+2|B|-2E} \left[1 + O(2^{E-|B|}) + O(2^{-E-|B|}) \right] \end{aligned} \quad (\text{A19})$$

A similar result holds when $P_A \neq I_A$ and $P_B = I_B$, with A and B exchanged.

(iii) $P_A = I_A$ and $P_B = I_B$. In this case the result is trivially $2^{4|A|+4|B|}$.

After combining all these contributions and including the multiplicity factors coming from the number of Pauli strings in each case, we obtain the final expression in Eq. (4) of the main text.

c. Eq. (5)

We now present the calculation details of Eq. (5) in the main text. Let us first recall the setup we use for this case. We consider a tripartite system A, B , and C . Since any tripartite stabilizer state can be transformed into a set of single-qubit states, Bell-pair states, and GHZ states via local Clifford unitaries, we consider initial state consisting

of g GHZ states shared among A , B , and C ; b_{AB} , b_{AC} , and b_{BC} Bell pairs shared between subsystems AB , AC , and BC , respectively, and f_A , f_B , f_C single-qubit states in each individual subsystem. Let us start by explicitly writing down a set of stabilizer generators for this state.

For the single-qubit states, we have

$$\mathbb{S}_A = \langle X_1, X_2, X_3, \dots, X_{f_A} \rangle, \quad (\text{A20})$$

and similarly for \mathbb{S}_B and \mathbb{S}_C . As the notation suggests, these are also the stabilizer subgroups on each individual subsystem. For the Bell-pair states shared between subsystem A and B , we have

$$L_{AB} = \langle X_{f_A+1} X_{|A|+f_B+1}, Z_{f_A+1} Z_{|A|+f_B+1}, \dots, X_{f_A+b_{AB}} X_{|A|+f_B+b_{AB}}, Z_{f_A+b_{AB}} Z_{|A|+f_B+b_{AB}} \rangle, \quad (\text{A21})$$

and similarly for L_{BC} and L_{AC} . Finally, for the GHZ state, we define

$$\begin{aligned} H_X &= \langle X_{|A|-g+1} X_{|A|+|B|-g+1} X_{|A|+|B|+|C|-g}, \dots \rangle \\ H_{AB} &= \langle Z_{|A|-g+1} Z_{|A|+|B|-g+1}, \dots \rangle \\ H_{AC} &= \langle Z_{|A|-g+1} Z_{|A|+|B|+|C|-g+1}, \dots \rangle \\ H_{BC} &= \langle Z_{|A|+|B|-g+1} Z_{|A|+|B|+|C|-g+1}, \dots \rangle. \end{aligned} \quad (\text{A22})$$

The set H_X , combined with any two of H_{AB} , H_{AC} , and H_{BC} , generates the GHZ states shared among subsystems A , B , and C .

Our approach of moving forward parallels that in the bipartite case. Namely, we decompose the stabilizer group into cosets of \mathbb{S}_{AB} and \mathbb{S}_C , the stabilizer subgroups of subsystem AB and C , respectively. Then we express the initial state in terms of the coset decomposition. The stabilizer group of subsystem \mathbb{S}_{AB} is given by

$$\mathbb{S}_{AB} = \langle \mathbb{S}_A, \mathbb{S}_B, L_{AB}, H_{AB} \rangle. \quad (\text{A23})$$

The stabilizer group of total system then can be decomposed as

$$\mathbb{S}_{ABC} = \underbrace{\mathbb{S}_{AB} \otimes \mathbb{S}_C \cup l_{AB}^1 \mathbb{S}_{AB} \otimes l_C^1 \mathbb{S}_C \cup \dots}_{4^{b_{AC}+b_{BC}+g} \text{ terms}}, \quad (\text{A24})$$

where l_{AB}^k and l_C^k are logical operators on AB and C as before. In this case, since we are dealing with initial state with a factorized structure, it is easy to directly identify the logical operators. For example, $\{l_{AB}^k\}$ consists of Pauli operators acting on $b_{AC} + b_{BC}$ Bell pairs, as well as Pauli operators acting on g GHZ states, hence $4^{b_{AC}+b_{BC}+g}$ operators in total. As before, to ensure elements across different cosets have the correct commutation relation as stabilizer group elements, we require (i) if $[l_{AB}^i, l_{AB}^j] = 0$, then $[l_C^i, l_C^j] = 0$; or (ii) if $\{l_{AB}^i, l_{AB}^j\} = 0$, then $\{l_C^i, l_C^j\} = 0$.

The average \bar{Y} can be written as

$$\begin{aligned} \bar{Y} &= \frac{1}{2^{5N}} \sum_{P \in P_N} \overline{\text{Tr}^4(P U_{AB} \otimes I_C \mathbb{S}_{ABC} U_{AB}^\dagger \otimes I_C)} \\ &= \frac{1}{2^{5N}} \sum_{P \in P_N} \sum_k \overline{\text{Tr}^4(P_{AB} U_{AB} l_{AB}^k \mathbb{S}_{AB} U_{AB}^\dagger)} \text{Tr}^4(P_C l_C^k \mathbb{S}_C), \end{aligned} \quad (\text{A25})$$

where $U_{AB} = U_A \otimes U_B$.

Now recall that $U_{AB} = U_A \otimes U_B$ in the current setup. Therefore, the term $\overline{\text{Tr}^4(P_{AB} U_{AB} l_{AB}^k \mathbb{S}_{AB} U_{AB}^\dagger)}$ has a similar factorization as in Eq. (A15). However, additional complications occur in this case, since, depending on l_{AB}^k , the set $l_{AB}^k \mathbb{S}_{AB}$ is further decomposed in different ways. In what follows, we use t_{ij} to represent the value of $\overline{\text{Tr}^4(P_{AB} U_{AB} l_{AB}^k \mathbb{S}_{AB} U_{AB}^\dagger)}$ in each case.

(1) $l_{AB}^k = I_{AB}$. We can decompose \mathbb{S}_{AB} into:

$$\mathbb{S}_{AB} = \underbrace{\mathbb{S}_A \otimes \mathbb{S}_B \cup u_1 \mathbb{S}_A \otimes v_1 \mathbb{S}_B \cup \dots}_{2^{2b_{AB}+g} \text{ terms}} \quad (\text{A26})$$

In this case, the quantity $\overline{\text{Tr}^4(P_{AB} U_{AB} l_{AB}^k \mathbb{S}_{AB} U_{AB}^\dagger)}$ factorizes into $\alpha_{P_A}(u_{k_1}, u_{k_2}, u_{k_3}, u_{k_4})$ and $\beta_{P_B}(v_{k_1}, v_{k_2}, v_{k_3}, v_{k_4})$ in a similar way as Eq. (A15). We can thus directly apply our previous results Eqs. (A8), (A16), (A18), and (A19), noticing that

$$\dim(\mathbb{S}_A) = f_A, \quad \dim(\mathbb{S}_B) = f_B, \quad \sum_{k_1, k_2, k_3, k_4} f_1 = 3 \cdot 2^{4b_{AB}+2g}. \quad (\text{A27})$$

- If $P_A \neq I_A, P_B \neq I_B$, we have:

$$t_{11} = 3 \cdot 2^{2f_A+2f_B+4b_{AB}+2g} \left(1 + 2 \cdot 2^{-2b_{AB}-g} + O(2^{-|A|+b_{AC}-b_{AB}}) + O(2^{-|B|+b_{BC}-b_{AB}}) \right) \quad (\text{A28})$$

- If $P_A = I_A, P_B \neq I_B$, we have:

$$t_{12} = 3 \cdot 2^{4|A|+2f_B} \left[1 + O(2^{b_{AB}+b_{BC}+g-|B|}) \right] \quad (\text{A29})$$

- If $P_A \neq I_A, P_B = I_B$, we have:

$$t_{13} = 3 \cdot 2^{2f_A+4|B|} \left[1 + O(2^{b_{AB}+b_{AC}+g-|A|}) \right] \quad (\text{A30})$$

- If $P_A = I_A, P_B = I_B$, we have:

$$t_{14} = 2^{4|A|+4|B|}. \quad (\text{A31})$$

(2) $l_{AB}^k \otimes l_C^k \in H_{AC} - I$. There are $N_2 := 2^g - 1$ terms, and we can decompose $l_{AB}^k \mathbb{S}_{AB}$ into:

$$l_{AB}^k \mathbb{S}_{AB} = \underbrace{\mathbb{S}_A \otimes v_1 \mathbb{S}_B + u_2 \mathbb{S}_A \otimes \mathbb{S}_B + u_3 \mathbb{S}_A \otimes v_3 \mathbb{S}_B \dots}_{2^{2b_{AB}+g} \text{ terms}} \quad (\text{A32})$$

To see that the decomposition above is correct, first notice that in this case l_{AB}^k are supported on subsystem A only, so there must be a term $u_2 \mathbb{S}_A \otimes \mathbb{S}_B$ where \mathbb{S}_B is left untouched. Secondly, since $H_{AB} \subset \mathbb{S}_{AB}$, for $l_{AB}^k \otimes l_C^k \in H_{AC} - I$, it must share a common Pauli- Z operator with an element in H_{AB} acting on the same GHZ state spanning A, B , and C . Thus, there will also be a term $\mathbb{S}_A \otimes v_1 \mathbb{S}_B$ where \mathbb{S}_A is recovered.

We can then immediately obtain the following results depending on the operator content of the Pauli string P on subsystem A and B , respectively.

- If $P_A \neq I_A, P_B \neq I_B$, we have:

$$t_{21} = 3 \cdot 2^{2f_A+2f_B+4b_{AB}+2g} \left(1 + 2 \cdot 2^{-2b_{AB}-g} + O(2^{-|A|+b_{AC}-b_{AB}}) + O(2^{-|B|+b_{BC}-b_{AB}}) \right) \quad (\text{A33})$$

- If $P_A = I_A, P_B \neq I_B$, we have:

$$t_{22} = 3 \cdot 2^{4|A|+2f_B} \left[1 + O(2^{-b_{AB}-b_{BC}-g-|B|}) \right] \quad (\text{A34})$$

- If $P_A \neq I_A, P_B = I_B$, we have:

$$t_{23} = 3 \cdot 2^{2f_A+4|B|} \left[1 + O(2^{-b_{AB}-b_{AC}-g-|A|}) \right] \quad (\text{A35})$$

- If $P_A = I_A, P_B = I_B$, we have:

$$t_{24} = 0, \quad (\text{A36})$$

since $I_{AB} \notin l_{AB}^k \mathbb{S}_{AB}$.

(3) $l_{AB}^k \otimes l_C^k \in \langle L_{BC}, H_{BC} \rangle - H_{BC}$. There are $N_3 := 2^{2b_{BC}+g} - 2^g$ terms. The reason we must exclude H_{BC} is that we have already included generators H_{AC} in case (2) discussed above, which, together with H_{AB} will generate H_{BC} already. In other words, elements in H_{BC} are already included in case (2) above, so we should avoid double counting. We can decompose $l_{AB}^k \mathbb{S}_{AB}$ into:

$$l_{AB}^k \mathbb{S}_{AB} = \underbrace{\mathbb{S}_A \otimes v_1 \mathbb{S}_B + u_2 \mathbb{S}_A \otimes v_2 \mathbb{S}_B + u_3 \mathbb{S}_A \otimes v_3 \mathbb{S}_B \dots}_{2^{2b_{AB}+g} \text{ terms}}, \quad (\text{A37})$$

since l_{AB}^k only acts on subsystem B . Similarly, we obtain the following results.

- If $P_A \neq I_A, P_B \neq I_B$, we have:

$$t_{31} = 3 \cdot 2^{2f_A+2f_B+4b_{AB}+2g} \left[1 + 2 \cdot 2^{-2b_{AB}-g} + O(2^{-|A|+b_{AC}-b_{AB}}) \right] \quad (\text{A38})$$

- If $P_A = I_A, P_B \neq I_B$, we have:

$$t_{32} = 3 \cdot 2^{4|A|+2f_B} \left[1 + O(2^{-b_{AB}-b_{BC}-g-|B|}) \right] \quad (\text{A39})$$

- If $P_A \neq I_A, P_B = I_B$, we have:

$$t_{33} = 0 \quad (\text{A40})$$

- If $P_A = I_A, P_B = I_B$, we have:

$$t_{34} = 0 \quad (\text{A41})$$

(4) $l_{AB}^k \otimes l_C^k \in \langle L_{AC}, H_{AC} \rangle - H_{AC}$, there are $N_4 := 2^{2b_{AC}+g} - 2^g$ terms. As before, since $l_{AB}^k \in H_{AC}$ has already been included in case (2) above, we should exclude them to avoid double counting. We can decompose $l_{AB}^k \mathbb{S}_{AB}$ into:

$$l_{AB}^k \mathbb{S}_{AB} = \underbrace{u_1 \mathbb{S}_A \otimes \mathbb{S}_B + u_2 \mathbb{S}_A \otimes v_2 \mathbb{S}_B + u_3 \mathbb{S}_A \otimes v_3 \mathbb{S}_B \dots}_{2^{2b_{AB}+g} \text{ terms}} \quad (\text{A42})$$

since in this case l_{AB}^k leaves subsystem B and hence \mathbb{S}_B untouched. Depending on the operator content of the Pauli string P on subsystem A and B , we obtain the following results.

- If $P_A \neq I_A, P_B \neq I_B$, we have:

$$t_{41} = 3 \cdot 2^{2f_A+2f_B+4b_{AB}+2g} \left[1 + 2 \cdot 2^{-2b_{AB}-g} + O(2^{-|B|+b_{BC}-b_{AB}}) \right] \quad (\text{A43})$$

- If $P_A = I_A, P_B \neq I_B$, we have:

$$t_{42} = 0 \quad (\text{A44})$$

- If $P_A \neq I_A, P_B = I_B$, we have:

$$t_{43} = 3 \cdot 2^{2f_A+4|B|} \left[1 + O(2^{-b_{AB}-b_{AC}-g-|A|}) \right] \quad (\text{A45})$$

- If $P_A = I_A, P_B = I_B$, we have:

$$t_{44} = 0 \quad (\text{A46})$$

(5) Finally, $l_{AB}^k \otimes l_C^k$ does not belong to any of the four cases listed above. There are $N_5 := 2^{2b_{AC}+2b_{BC}+2g} - 2^{2b_{AC}+g} - 2^{2b_{BC}+g} + 2^g$ terms. In this case, l_{AB}^k does not leave either of \mathbb{S}_A and \mathbb{S}_B invariant, and the decomposition of $l_{AB}^k \mathbb{S}_{AB}$ reads:

$$l_{AB}^k \mathbb{S}_{AB} = \underbrace{u_1 \mathbb{S}_A \otimes v_1 \mathbb{S}_B + u_2 \mathbb{S}_A \otimes v_2 \mathbb{S}_B + u_3 \mathbb{S}_A \otimes v_3 \mathbb{S}_B \dots}_{2^{2b_{AB}+g} \text{ terms}} \quad (\text{A47})$$

- If $P_A \neq I_A, P_B \neq I_B$, we have:

$$t_{51} = 3 \cdot 2^{2f_A+2f_B+4b_{AB}+2g} \left(\begin{aligned} &1 + 2 \cdot 2^{-2b_{AB}-g} + \\ &+ O(2^{-|A|-b_{AB}-b_{AC}-g}) + O(2^{-|B|-b_{BC}-b_{AB}-g}) \end{aligned} \right) \quad (\text{A48})$$

- If $P_A = I_A, P_B \neq I_B$, we have:

$$t_{52} = 0 \quad (\text{A49})$$

- If $P_A \neq I_A, P_B = I_B$, we have:

$$t_{53} = 0 \quad (\text{A50})$$

- If $P_A = I_A, P_B = I_B$, we have:

$$t_{54} = 0 \quad (\text{A51})$$

The \bar{Y} is then expressed in Eq. (A52):

$$\begin{aligned} & 2^{5|A|+5|B|+5|C|} \cdot 2^{-4|C|} \cdot 2^{-|C|+b_{AC}+b_{BC}+g} \cdot \bar{Y} \\ &= t_{11} + N_2 t_{21} + N_3 t_{31} + N_4 t_{41} + N_5 t_{51} \\ &+ (4^{|B|} - 1) [t_{12} + N_2 t_{22} + N_3 t_{32} + N_4 t_{42} + N_5 t_{52}] \\ &+ (4^{|A|} - 1) [t_{13} + N_2 t_{23} + N_3 t_{33} + N_4 t_{43} + N_5 t_{53}] \\ &+ (4^{|A|} - 1)(4^{|B|} - 1) [t_{14} + N_2 t_{24} + N_3 t_{34} + N_4 t_{44} + N_5 t_{54}] \end{aligned} \quad (\text{A52})$$

In the above summation, the prefactor $2^{-|C|+b_{AC}+b_{BC}+g}$ comes from the size of each coset $|L_C^k \mathbb{S}_C|$. We observe that some terms may include contributions of the form $t_{41} = 3 \cdot 2^{2f_A+2f_B+4b_{AB}+2g} [1+2 \cdot 2^{-2b_{AB}-g} + O(2^{-|B|+b_{BC}-b_{AB}})]$, which raises concerns about whether these subleading terms $O(2^{-|B|+b_{BC}-b_{AB}})$ can be neglected when the entanglement is large. However, we can verify that the number of t_{41} is N_4 , while the number of t_{51} is N_5 , and we have $N_4/N_5 \approx 2^{-2b_{BC}-g}$. Therefore, the subleading terms contributes $O(2^{-|B|-b_{BC}-b_{AB}-g})$ to the final result.

Appendix B: An example of the decomposition of the stabilizer group

In this section, we give a concrete example of the coset decomposition of a stabilizer group that has been widely used in this work. Consider a 5-qubit GHZ state:

$$\frac{1}{\sqrt{2}} (|00000\rangle + |11111\rangle) \quad (\text{B1})$$

The elements of the corresponding stabilizer group, denoted as \mathbb{S}_{AB} , are listed in Table I. We partition the system into two subsystems: subsystem A consisting of the first three qubits and subsystem B consisting of the remaining two qubits. The reduced density matrices for these subsystems are given by Eq. (B2):

$$\rho_A = \frac{1}{2^3} (III_A + IZZ_A + ZIZ_A + ZZI_A), \quad \rho_B = \frac{1}{2^2} (II_B + ZZ_B) \quad (\text{B2})$$

Defining the stabilizer subgroups as

$$\mathbb{S}_A := \{III_A, IZZ_A, ZIZ_A, ZZI_A\}, \quad \mathbb{S}_B := \{II_B, ZZ_B\}, \quad (\text{B3})$$

we observe that $\mathbb{S}_A \otimes \mathbb{S}_B$ forms a subgroup of \mathbb{S}_{AB} . Consequently, \mathbb{S}_{AB} can be decomposed into this subgroup and its corresponding cosets, as expressed in Eq. (B4):

$$\mathbb{S}_{AB} = \mathbb{S}_A \otimes \mathbb{S}_B \cup a_1 \mathbb{S}_A \otimes b_1 \mathbb{S}_B \cup a_2 \mathbb{S}_A \otimes b_2 \mathbb{S}_B \cup a_3 \mathbb{S}_A \otimes b_3 \mathbb{S}_B \quad (\text{B4})$$

The states stabilized by \mathbb{S}_A form a stabilizer code defined on subsystem A , specifically the code space spanned by $\{|000\rangle_A, |111\rangle_A\}$. Similarly, the stabilizer code for subsystem B is spanned by $\{|00\rangle_B, |11\rangle_B\}$. The operators a_k and b_k correspond to the logical operators of the stabilizer codes on A and B , respectively. Notably, these logical operators are combined in a manner that ensures all $a_k \otimes b_k$ commute with one another.

$S_A \otimes S_B$	$XXXS_A \otimes XXS_B$	$IIZS_A \otimes ZIS_B$	$-XXYS_A \otimes YXS_B$
IIII	XXXXX	IIZZI	-XXYYX
IZZII	-XYYXX	IZIZI	-XYYXX
ZZIII	-YYXXX	ZZZZI	YYYYX
ZIZII	-YXYXX	ZIIZI	-YXXYX
IIIZZ	-XXXYY	IIZIZ	-XXXYY
IZZZZ	XYYYY	IZIIZ	-XYYXX
ZZIZZ	YXYYY	ZZZIZ	YYYYX
ZIZZZ	YXYYY	ZIIZZ	-YXXYX

TABLE I. Stabilizer group of 5-qubit GHZ state and its decomposition.

Appendix C: Factorized unitary acting on three subregions

In this section, we consider the effect of a factorized unitary acting on all three subregions of a tripartite state: $U = U_A \otimes U_B \otimes U_C$. In this case, the final result reads:

$$\begin{aligned} \bar{Y} = & 4 \cdot 2^{-N} [1 + 3 \cdot 2^{-2b_{AB}-2b_{AC}-2g} + 3 \cdot 2^{-2b_{AB}-2b_{BC}-2g} + 3 \cdot 2^{-2b_{AC}-2b_{BC}-2g} \\ & + \frac{3}{2} \cdot 2^{-2b_{AB}-2b_{AC}-2b_{BC}-2g} + \frac{9}{2} \cdot 2^{-2b_{AB}-2b_{AC}-2b_{BC}-3g}] \end{aligned} \quad (\text{C1})$$

where once again subleading corrections are of the order $O(2^{-|A|}, 2^{-|B|}, 2^{-|C|})$. Similarly to the bipartite result Eq. (4) in the main text, we find that the resulting state also achieves maximal amount of magic, provided that the subsystems are sufficiently entangled. Interestingly, this does require that the A , B , and C are pairwise entangled. As Eq. (C1) suggests, if $A&B$, $B&C$ are highly entangled while $A&C$ are not entangled (i.e. b_{AB}, b_{BC} is large, but b_{AC} is zero), the average \bar{Y} still approaches that of a Haar random state.

As a consistency check, we consider a special case of Eq. (C1), namely, when only $A&B$ are entangled, and C is not entangled with AB . In this case, we can check that the average \bar{Y} coincides with a product of Eq. (4) in the main text for the bipartite case and a single Haar random state on C , which is consistent with our previous results.

We now detail the calculation of Eq. (C1). Our strategy parallels that used for the bipartite case. We first decompose the stabilizer group for the system S_{ABC} as

$$S_{ABC} = \underbrace{S_A \otimes S_B \otimes S_C \cup a_1 S_A \otimes b_1 S_B \otimes c_1 S_C \cup \dots}_{d := 2^{2b_{AB}+2b_{AC}+2b_{BC}+3g} \text{ terms}} \quad (\text{C2})$$

where $a_k \otimes b_k \otimes c_k \in \langle L_{AB}, L_{BC}, L_{AC}, H_X, H_{AB}, H_{BC} \rangle$. Notice, however, since our initial state now factorizes into single-qubit, Bell pair and GHZ states, the logical operators $\{a_k, b_k, c_k\}$ have more structures. For example, the $2^{2b_{AB}+g}$ elements in $\langle L_{AB}, H_{AB} \rangle$ are only supported on subsystems A and B , hence there are $d_C := 2^{2b_{AB}+g}$ terms in the coset decomposition (C2) that have the same c_k 's. Similarly, there are $d_A := 2^{2b_{BC}+g}$ cosets with the same a_k 's, and $d_B := 2^{2b_{AC}+g}$ cosets with the same b_k 's.

After applying $U := U_A \otimes U_B \otimes U_C$ and averaging over Haar random unitaries, we obtain:

$$\bar{Y} = \frac{1}{2^{5N}} \sum_{P \in P_N} \sum_{k_1, k_2, k_3, k_4} \alpha_{P_A}(a_{k_1}, a_{k_2}, a_{k_3}, a_{k_4}) \beta_{P_B}(b_{k_1}, b_{k_2}, b_{k_3}, b_{k_4}) \gamma_{P_C}(c_{k_1}, c_{k_2}, c_{k_3}, c_{k_4}). \quad (\text{C3})$$

Now, depending on the operator contents of the Pauli string P on subsystems A , B and C (identity or not), we use Eq. (A7) and Eq. (A8) to evaluate the above expression. We give one example here. Consider when $P_A \neq I_A$, $P_B \neq I_B$, and $P_C \neq I_C$, using Eq. (A7) and Eq. (A8), we expand Eq. (C3) as follows:

$$\begin{aligned} & \overline{\text{Tr}^4(PUS_{ABC}U^\dagger)} \\ & = 2^{2f_A+2f_B+2f_C} (3d^2 + 6dd_A + 6dd_B + 6dd_C + 6d \cdot 2^g) \\ & \quad + O(2^{3f_A+2f_B+2f_C-2|A|} d^2) + O(2^{2f_A+3f_B+2f_C-2|B|} d^2) \\ & \quad + O(2^{2f_A+2f_B+3f_C-2|C|} d^2) + O(2^{3f_A+3f_B+3f_C-2|A|-2|B|-2|C|} d^3) \\ & = 3 \cdot 2^{2f_A+2f_B+2f_C} d \left(d + 2d_A + 2d_B + 2d_C + 2 \cdot 2^g + O(2^{-|A|}) + O(2^{-|B|}) + O(2^{-|C|}) \right), \end{aligned} \quad (\text{C4})$$

where $d := 2^{2b_{AB}+2b_{AC}+2b_{BC}+3g}$ is the total number of cosets. The first line can be obtained when only leading order terms, namely, the first line in Eq. (A8) is considered. Then we need to calculate the following summations over $\{k_1, k_2, k_3, k_4\}$, constrained by products of δ -functions:

$$\sum_{k_1, k_2, k_3, k_4} \delta_2(a_{k_1}, a_{k_2}) \delta_2(a_{k_3}, a_{k_4}) \delta_2(b_{k_1}, b_{k_2}) \delta_2(b_{k_3}, b_{k_4}) \delta_2(c_{k_1}, c_{k_2}) \delta_2(c_{k_3}, c_{k_4}) = d^2 \quad (\text{C5})$$

$$\sum_{k_1, k_2, k_3, k_4} \delta_2(a_{k_1}, a_{k_2}) \delta_2(a_{k_3}, a_{k_4}) \delta_2(b_{k_1}, b_{k_2}) \delta_2(b_{k_3}, b_{k_4}) \delta_2(c_{k_1}, c_{k_3}) \delta_2(c_{k_2}, c_{k_4}) = dd_C \quad (\text{C6})$$

$$\sum_{k_1, k_2, k_3, k_4} \delta_2(a_{k_1}, a_{k_2}) \delta_2(a_{k_3}, a_{k_4}) \delta_2(b_{k_1}, b_{k_3}) \delta_2(b_{k_2}, b_{k_4}) \delta_2(c_{k_1}, c_{k_4}) \delta_2(c_{k_2}, c_{k_3}) = 2^g d \quad (\text{C7})$$

This is where we need to be careful with the number of cosets having identical a_k 's, b_k 's, or c_k 's. The first summation is straightforward, if we fix an arbitrary $a_{k_1} \otimes b_{k_1} \otimes c_{k_1}$, then we find no more constraints except for $a_{k_2} \otimes b_{k_2} \otimes c_{k_2} = a_{k_1} \otimes b_{k_1} \otimes c_{k_1}$ and $a_{k_3} \otimes b_{k_3} \otimes c_{k_3} = a_{k_4} \otimes b_{k_4} \otimes c_{k_4}$, so the summation over k_1 and k_3 can be chosen independently, leading to d^2 .

For the second summation, because of the factors $\delta_2(a_{k_1}, a_{k_2})$, $\delta_2(b_{k_1}, b_{k_2})$, we have $a_{k_1} \otimes b_{k_1} \otimes c_{k_1} = a_{k_2} \otimes b_{k_2} \otimes c_{k_2}$, similarly we have $a_{k_3} \otimes b_{k_3} \otimes c_{k_3} = a_{k_4} \otimes b_{k_4} \otimes c_{k_4}$. And considering further the factor $\delta_2(c_{k_1}, c_{k_3})$, we find once we fix $a_{k_1} \otimes b_{k_1} \otimes c_{k_1}$, there are only $d_C = 2^{2b_{AB}+g}$ choices for $a_{k_3} \otimes b_{k_3} \otimes c_{k_3}$, thus the summation is dd_C .

For the third summation, once we fix $a_{k_1} \otimes b_{k_1} \otimes c_{k_1}$, because of the factor $\delta_2(a_{k_1}, a_{k_2})$, we need $a_{k_2} \otimes b_{k_2} \otimes c_{k_2} \in a_{k_1} \otimes b_{k_1} \otimes c_{k_1} \cdot \langle L_{BC}, H_{BC} \rangle$; because of the factor $\delta_2(b_{k_1}, b_{k_3})$, we can choose $a_{k_3} \otimes b_{k_3} \otimes c_{k_3} \in a_{k_1} \otimes b_{k_1} \otimes c_{k_1} \cdot \langle L_{AC}, H_{AC} \rangle$; considering further the factor $\delta_2(c_{k_2}, c_{k_3})$, we can only choose $a_{k_2} \otimes b_{k_2} \otimes c_{k_2} \in a_{k_1} \otimes b_{k_1} \otimes c_{k_1} \cdot \langle H_{BC} \rangle$. Furthermore, once $a_{k_2} \otimes b_{k_2} \otimes c_{k_2}$ is fixed, $a_{k_3} \otimes b_{k_3} \otimes c_{k_3}$ is also determined, because $\delta_2(c_{k_2}, c_{k_3})$ implies that $a_{k_3} \otimes b_{k_3} \otimes c_{k_3}$ can only be obtained by acting on $a_{k_1} \otimes b_{k_1} \otimes c_{k_1}$ with stabilizer group element of the same GHZ state as in $a_{k_2} \otimes b_{k_2} \otimes c_{k_2}$. Finally, $a_{k_4} \otimes b_{k_4} \otimes c_{k_4}$ is also fully fixed by the δ -functions. Therefore, there are only two independent summations in the choices for k_1 and the GHZ state in H_{BC} , leading to the final result $2^g d$.

After similar analysis, we obtain:

$$\begin{aligned} & \overline{\text{Tr}^4(PUS_{ABC}U^\dagger)} \\ = & \begin{cases} 3 \cdot 2^{2f_A+2f_B+2f_C} d(d+2d_A+2d_B+2d_C+2 \cdot 2^g), & P_A \neq I_A, P_B \neq I_B, P_C \neq I_C \\ 2^{4|A|+2f_B+2f_C} (3d_A^2+6d_A), & P_A = I_A, P_B \neq I_B, P_C \neq I_C \\ 3 \cdot 2^{4|A|+4|B|+2f_C}, & P_A = I_A, P_B = I_B, P_C \neq I_C \\ 2^{4|A|+4|B|+4|C|}, & P_A = I_A, P_B = I_B, P_C = I_C \end{cases}. \end{aligned} \quad (\text{C8})$$

The subleading corrections are of the order $O(2^{-|A|}, 2^{-|B|}, 2^{-|C|})$ in each line. Cases not listed in Eq. (C8) are similar. After combining all terms together, we obtain Eq. (C1).

Appendix D: Magic injection with shallow-depth brickwork circuits

In this section, we replace the Haar random unitary gate acting on A with a shallow-depth brickwork circuit. First, we still consider the initial state shown in Fig. 1(d) of the main text, followed by one layer of local \bar{g} gates acting on subregion A . Since the initial state factorizes into single-qubit states and Bell-pair states, the average \bar{Y} also factorizes into a product of contributions from single-qubit and Bell pair states. Thus, it is easy to see that, $\bar{Y} \propto 2^{-E}$ still holds true in this case.

However, if U_A is not Haar random, the specific choice of initial state in Fig. 1(d) is no longer the most generic one. To construct the most general stabilizer initial state with tunable entanglement, notice that since any bipartite stabilizer state is local-unitary equivalent to the state in Fig. 1(d), we can simply recover a generic stabilizer state by acting on Fig. 1(d) with random Clifford unitaries $U_A^{\text{Cliff}} \otimes U_B^{\text{Cliff}}$. Since U_B^{Cliff} commutes with subsequent magic injection gates supported on A and leaves Y invariant, we can simply apply U_A^{Cliff} . We then consider brickwork circuits of varying depths and gate ranges, as summarized in Fig. 7. We then numerically compute the average \bar{Y} corresponding to each circuit architecture, and the results are shown in Fig. 8. We find that the qualitative picture of our analytical result is still valid for the brickwork circuit, in that the average \bar{Y} decays exponentially with E . However, notice that for extremely shallow depths (single layer and two layers), the curve bends upward and saturates, which indicates magic injection that is below capacity. As the circuit depth increases, the behavior of \bar{Y} approaches that of a Haar random U_A .

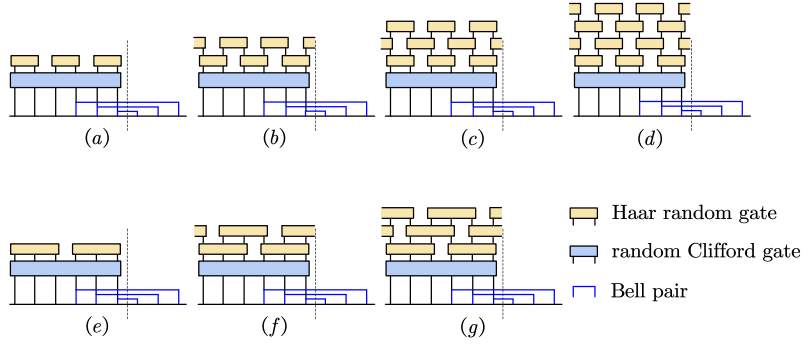


FIG. 7. The circuits used to simulate the case where the gate acting on A is not sampled from a global Haar ensemble. The blue lines represent Bell pairs. The blue bricks represent unrelated random Clifford gates, and the yellow bricks represent unrelated random magical gates.

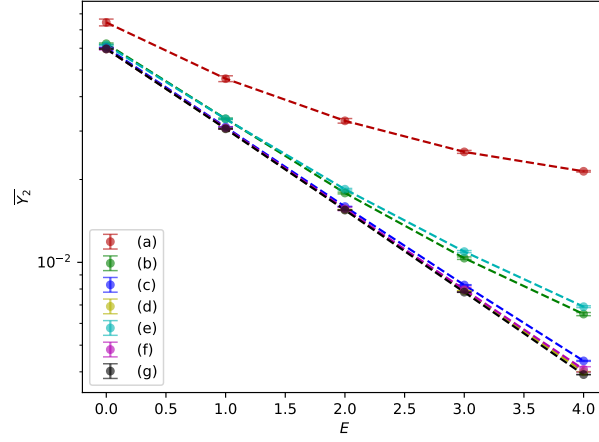


FIG. 8. Numerical results for \bar{Y} under brickwork circuits of varying depths and gate ranges, as depicted in Fig. 7.

Appendix E: Simulation method

In this section, we briefly discuss the numerical simulation method we used. We use two different methods for numerically evaluating the average \bar{Y} . The first one is a brute-force evaluation according to the definition of Y . However, this requires a direct enumeration of all 4^N Pauli strings, which can be time-consuming for larger system sizes. We thus adopt a second method, which is inspired by our analytical calculations to avoid summing over exponentially many Pauli strings. According to Eq. (A12), there are only four different values for $\alpha_{P_A}(a_k, a_k, a_k, a_k)$, depending on whether $P_A = I_A$ and $a_k = I_A$. Therefore, we only need to evaluate the corresponding α 's to efficiently compute the average \bar{Y} . Similarly, there are four possible contributions from different P in Eq. (A15), so we can simply simulate these values to obtain an unbiased estimate for \bar{Y} .